# Experimental assessment of wheel/rail interaction force with rolling noise analysis

Pierre-Emile Chartrain, Pierre-Olivier Mattei, Estelle Bongini

ACOUSTICS 2012

# Experimental assessment of wheel/rail interaction force with rolling noise analysis

P.-E. Chartrain[a], P.-O. Mattei[b] and E. Bongini[a]

[a]Innovation & Recherche SNCF, 40 Avenue des terroirs de France, 75012 Paris, France
[b]LMA, CNRS, UPR 7051, Aix-Marseille Univ, Centrale Marseille, 31 chemin Joseph Aiguier, F-13402 Marseille Cedex 20, France
pierre-emile.chartrain@sncf.fr

The main source of noise from railway at conventional speeds is rolling noise. The wheel and the rail surfaces are not perfectly smooth, but contain small-amplitude roughness. This roughness causes vibration of the wheel and rail which radiate noise. Within the LECAV project (LECture Acoustique de la Voie, i.e. Acoustic reading of railway track) a method is developed to use the sound radiated by the wheel and the rail to characterize acoustics parameters of wheel track system during train running. These parameters will allow estimating rail roughness spectrum and potentially track decay rate. This method requires to have control over the acoustic radiation of the wheel and rail in order to estimate the interaction force between the two elements in the contact zone. The first part of this communication is devoted to the presentation of a measurement campaign that has been carried out on a test train parked on a railway track. The second part of the paper deals with the post-processing method. Results of the estimated excitation force from the simultaneous measurement of the acoustic sound pressure and vibration of the wheel are compared to the measured one to validate the method

# 1 Introduction

## 1.1 Context

Rolling noise is the main source for railway noise for speeds between 50 to 300 km/h. It is induced by the interaction between the rail and the wheel as the train runs on a track. The wheel and the rail surfaces are not perfectly smooth, but possess small-irregularities called roughness. This roughness induces vibration of the wheel and the rail which radiate noise. The wheel is the primary contributor to the radiated noise for the frequencies range from 2 kHz to 5 kHz; below these frequencies, the track (sleeper and rail) is the predominant source of noise [1].

The European Directive 2002/49/EC [2] imposes to build a cartography of the acoustic radiation of the railway network. The roughness is one of the main parameters to assess the environmental noise and to establish this cartography. An on-board system developed to monitor the track roughness is therefore necessary. Moreover, these measurements will allow optimizing the maintenances of the network.

## 1.2 Approach

The rolling noise theory proposed by Remington in the eighties [3] (and implemented in TWINS[1]) demonstrate that this noise results of the combination of the roughness spectra of the wheel and the rail. The method developped in LECAV proposes to use an inverse process which consists in the determination of the roughness based on the rolling noise measurement (see Figure 1)

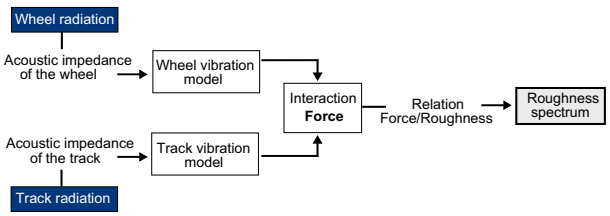


Figure 1: Model for roughness spectrum assessment.

The sound radiated by the wheel and the rail during train pass-by contains information on the vibration behaviour of the wheel track system. Vibrations of the wheel and the rail depend on the interaction force between them both. This force will then allow estimating the rail roughness spectrum and the dynamic behaviour of the track. One of the main steps of this method reside in the determination of the interaction force. It is therefore necessary to measure the acoustic impedance and vibration mobility (transfert function between vibration velocity and input force) of the wheel and the track. A measurement campaign has been carried out to model and validate the vibroacoustic behaviour (acoustic impedance and mobility) of the wheel-track system.

[1] Track Wheel Interaction Noise Software

# 2 Measurements setup

In this paper, only the analysis dedicated to the wheel will be presented. The measurement has been carried out on a test train parked on a railway track, in environemental conditions close to the operational uses. Indeed, the preload of the train on the wheel, the mobility of the track in contact point between the wheel and the rail, the acoustic effect of the ground and the train's body are taken into account (see Figure 2).

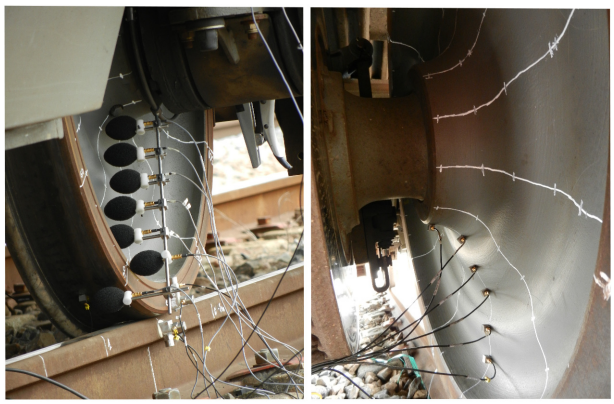

Figure 2: Acoustic and vibratory acquisition system.

To specify the sound impedance of the wheel, the vibration and the acoustic pressure at eight radial positions and twelve angular positions have been measured simultaneously for the frequency range [100 Hz - 6000 Hz]. The density of the mesh allows identifying vibration modes shapes until around 5000 Hz. Figure 3 shows the measurement setup of the wheel: The positions one at six, seven and eight are respectively located on the web, on the tyre and on the tread of the wheel. The excitation force can not be applied at the contact point between the wheel and the rail, hence it is applied at 300° for axial (on the tyre) and radial (on the tread) directions. For each position, acoustic and acceleration acquisitions are averaged on all the ten hammer excitations. One microphone and two accelerometers at fixed location during the acquisitions confirm the repeatability of the set of measures on the wheel.

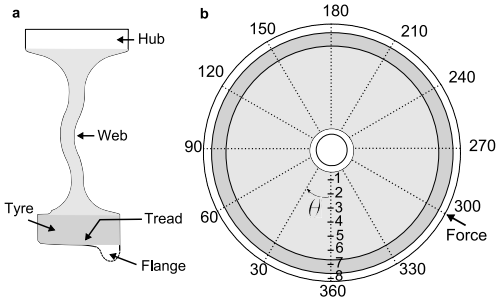


Figure 3: (**a**) Cross-section of 890 mm monobloc Wheel, (**b**) accelerometers and microphones positions.

# 3 Vibroacoustic behaviour of the wheel

Firstly, acoustic and velocity energy distribution are studied with a macroscopic point of view. Secondly, the modal characteristics of the wheel are observed.

## 3.1 Energy distribution

The acoustic ($H_a$) and vibration ($H_v$) amplitudes distribution on the radius of the wheel, for each radial positions $i$, are shown in Figure 4. The amplitudes are the RMS[2] values of the transfer functions averaged for each angle $\theta$ (see Figure 3) given by:

$$ {}_iH_a = \sum_{j=1}^{j=12} \sqrt{\left( \frac{1}{N} \sum_{k=0}^{N-1} \left| \frac{{}_iP_{\theta_j}[k]}{F_j[k]} \right|^2 \right)} \quad (1) $$

$$ {}_iH_v = \sum_{j=1}^{j=12} \sqrt{\left( \frac{1}{N} \sum_{k=0}^{N-1} \left| \frac{{}_iv_{\theta_j}[k]}{F_j[k]} \right|^2 \right)} \quad (2) $$

where $P$ is the pressure, $v$ is the velocity, $F$ is the force and $N$ is the sample number.

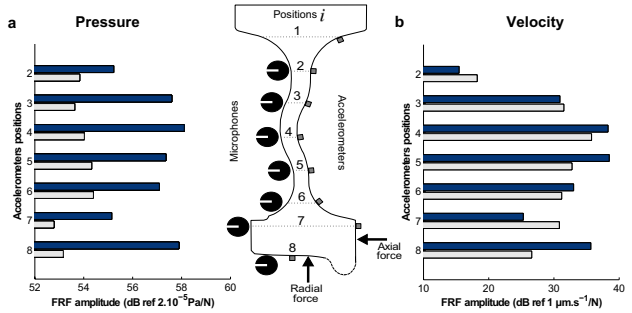


Figure 4: RMS FRF amplitudes; (**a**) acoustic ($H_a$), (**b**) vibration ($H_v$) on the web of the wheel for a radial (■) and axial (○) excitation.

Figure 4 shows that a coupling exists between the radial and axial excitation. In fact for the radial excitation, normal vibration of the web of the wheel is most important than for an axial excitation due to complex geometry of the wheel. The same effect is noticeable for pressure levels. The maxima of vibration and pressure appear at the centre of the web.

[2]Roots mean square

## 3.2 Modes of vibration

All finite structures have a serie of resonances and associated natural frequencies. The steel railway wheel has a very small damping. Its vibration behaviour is particularly characterised by its resonances. Each resonance frequency corresponds to a mode shape. The wheel mode shapes are alike at those of a flat circular plate. This modes can be categorized by the number of nodal diameters and nodal circles. For example, in Figure 5 the left sub-figure shows a mode with one nodal diameter and zero nodal circle, the right one shows a mode with six nodal diameters and one nodal circle. Table 1 lists the measured natural frequencies.

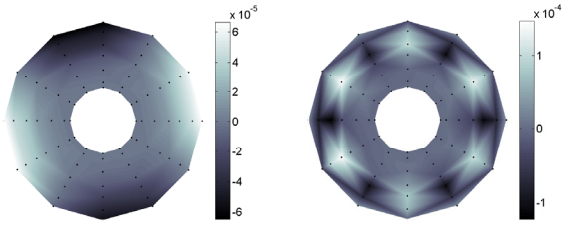

(a) $f$=372 Hz (b) $f$=4870 Hz

Figure 5: Measured modes shapes deformation of the wheel in velocity (m.s$^{-1}$/N).

| $n$ | Zero nodal-circle | One nodal-circle | Radial | Two nodal-circle |
|---|---|---|---|---|
| 0 | - | 251 | - | 2774 |
| 1 | 138 | - | - | - |
| 2 | 372 | 2353 | 1759 | 3787 |
| 3 | 992 | 2934 | 2415 | 4465 |
| 4 | 1789 | 3561 | 3178 | 5189 |
| 5 | 2697 | 4262 | 4050 | 4642 |
| 6 | 3694 | 4870 | - | 5084 |
| 7 | 4638 | - | - | - |

Table 1: Natural frequencies measured in Hertz for 890 mm monobloc wheel, $n$ is the number of nodal diameters.

# 4 Experimental based assessment of the force

The assessment of the force will be carried out only at the natural frequencies of the wheel. At these frequencies, we assumes that the signal to noise ratio is sufficiently high to make the aerodynamic noise contribution negligible.

## 4.1 Method

The method used to estimate the force at contact point between the wheel and the rail is explained in Figure 6. First, the acoustic pressure at a point $i$ is measured in near field of the surface of the wheel. When the LECAV system will be installed on the train, only this data will be available. From the pressure data, the resonance frequencies are detected at the peaks. Then, the modal parameters are calculated for each resonance frequency. Using the acoustic impedance,

the velocity at a point $i$ can be calculated. Finally, from the mobility of the wheel between the excitation force and each point $i$ on the web, the force can be evaluated.

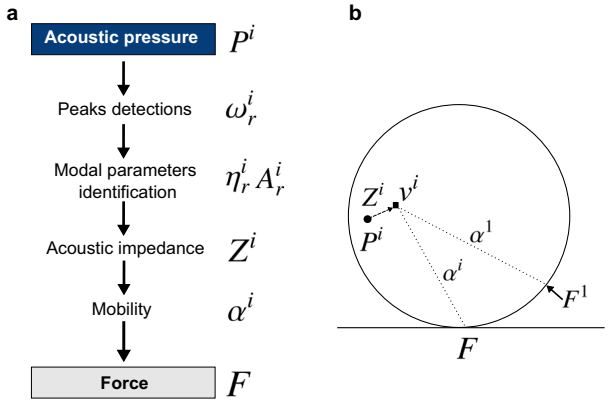


Figure 6: (**a**) Force assessment method, (**b**) sketch of transfer functions combination.

### Natural frequencies identification at peaks

The frequency range in which the natural frequencies is detected depends on the speed of the train and the roughness wavelength. In fact, the pass by of the wheel on the rail with the spatial roughness wavelength $\lambda$ at the speed $V$ generates vibration in the wheel and the rail at frequency $f$

$$f = \frac{V}{\lambda} \tag{3}$$

The spatial wavelength associated to the natural frequency depends then on the speed. A speed of 200 km/h allows reading the roughness with the wavelength between 9 and 300 mm. In this case, the frequency range where the peack are read spreads between 185 Hz and 6176 Hz. Typical wavelength of roughness ascribed at rolling noise are between 8 and 500 mm [4]. This speed allows detecting a major part of conventional roughness wavelength. The detection of peaks are based on three parameters:

- level emergences on the global signal,
- local emergences on the mean level of short samples of signal,
- the number of modes.

The two first parameters are iterative thresholds. The first parameter detects the high emergences, the second parameter selects the weak emergences between the strongest peaks; and the number of modes, chosen by the user, allows stopping the iterative process. Figure 8.a. shows the detected peaks on the pressure signal with thirteen modes.

### Modal parameters identification

The small damping of the modes allows clear separation between each mode. Each single mode can be sequentially analysed in the frequency range of interest. Each natural mode noted $r$ is given by its pulsation $\omega_r$, its damping $\eta_r$, and its amplitude $A_r$. All these quantities are determined by using the circle-fit method in Nyquist plot [5]. The samples data in the vicinity of resonances produce an exact circle in the Nyquist plot. For each resonance frequency, the theoretical circle is built and the modal parameters are estimated from the properties of the Nyquist circle.

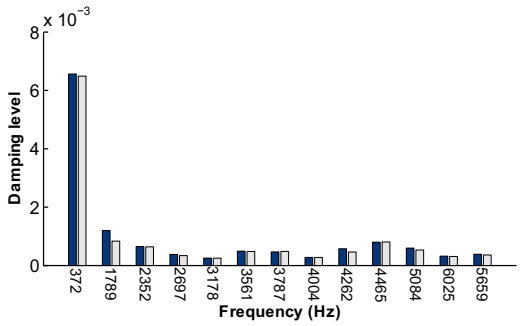


Figure 7: Damping level; from the pressure (■), from the velocity (■).

Figure 8.a shows the measured pressure in near field at one point[3] of the web and Figure 8.b shows the velocity at the same point. The pressure behaviour is in good agreement with the velocity behaviour, particularly for the damping level that is almost the same for both, see Figure 7. Hence, at the natural frequencies, the damping identified from the pressure can be associated to the damping of the wheel.

### Acoustic impedance

The resonance frequencies and the damping are now estimated, but it is necessary to determined the level relation between the pressure and the velocity for computing the amplitude value of the velocity. We use the acoustic impedance noted $Z_r^i$ only at the $r^{th}$ natural frequencies of the wheel at location $i$:

$$Z_r^i = \frac{P_r^i}{v_r^i} \tag{4}$$

Then, with the modal superposition theory, the modal parameters and this relation, the velocity can be written

$$v^i(\omega) = \sum_{r=1}^{N} \frac{A_r^i}{\omega_r^2 - \omega + j\eta_r\omega_r^2} \frac{1}{Z_r^i}, \tag{5}$$

where $N$ is the number of natural frequencies detected. Figure 8.b shows the velocity $v$ computed and measured at the radial position 4 and at angle 120°.

The calculated velocity from the equation (5) is very close to the measured velocity only around natural frequencies. The identification of modal parameters and the evaluation of acoustic impedance from the pressure are validated.

### Vibration response

The transfer function $\alpha$ between the velocity $v$ at one point $i$ and the interaction force $F$ (see Figure 6.b) at each mode is defined by

$$\alpha_r^i = \frac{v_r^i}{F}. \tag{6}$$

Then from the velocity, the force can be estimated.

[3] The point is at position 4 and at 60° (Figure 3)

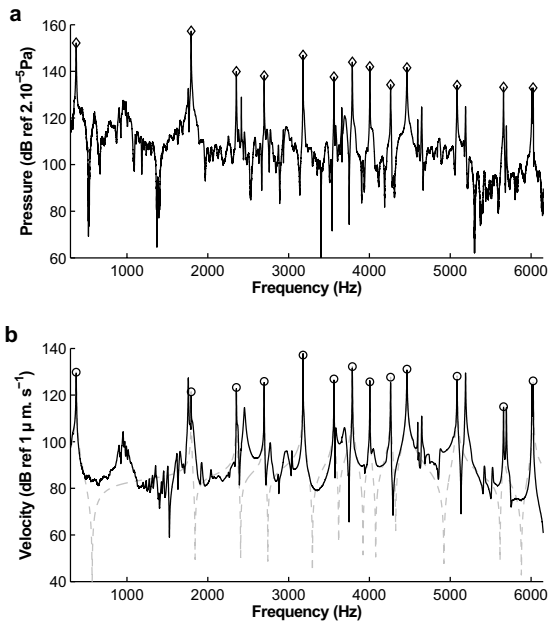


Figure 8: (**a**) Measured pressure (—) and peaks detections (◇) for $N$=13. (**b**) Velocity: measurement (—), model (– ○ –).

### Force

Finally, the interaction force between the wheel and the rail from the pressure at one point $i$ for each resonances $r$ is given by

$$F_r = \frac{P_r^i}{\alpha_r^i Z_r^i} \tag{7}$$

## 4.2 Results

An example of estimated experimental excitation force $F^1$ based on the pressure at point 4 on an angle of 60°, compared to the measured force (with a force sensor on the impact hammer), is given in Figure 9.

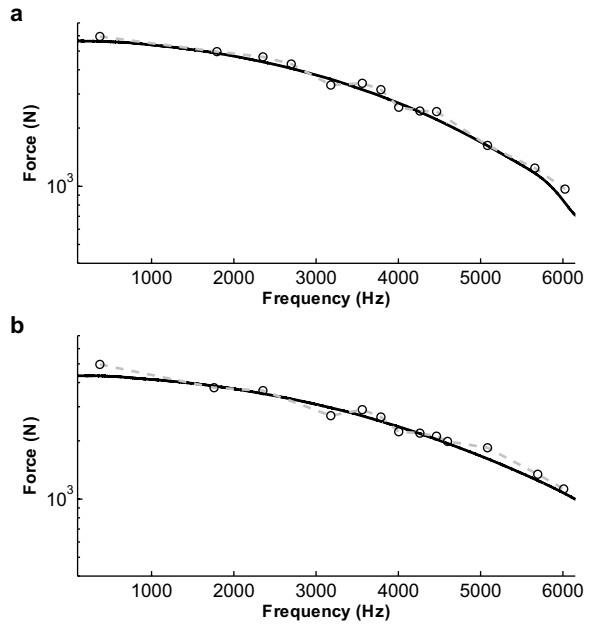


Figure 9: Force $F^1$: measurement (—), model (– ○ –); (**a**) axial excitation, (**b**) radial excitation.

Figure 9 shows that, the predicted force is close to the measured force and the force can be correctly estimated on the large frequency range with linear interpolation. The method to assess the force is validated through the measurements.

### Optimization of assessed force

In the following, the measured pressure and the velocity are normalized by the excitation force. If the number of detection $N$ is reduced, only the high emergences of pressure signal can be detected and there amplitude levels are acceptable enough to allow a better robustness analysis. The assessment of the force behaviour is however reduced on the frequency. But by using several microphones, the force can be estimated for a larger frequency range. Indeed, the positioning of the microphones on several locations on the web of the wheel allows to detect a mode depending on its mode shape (minimal and maximal of vibration depending on radial and the angle positions). Figure 10 illustrates the different mode detections from all radial positions (5 positions) on the web of the wheel at 1 angle. The number of mode $N$ by positions is fixed at 10. In this configuration, 14 modes are finally detected.

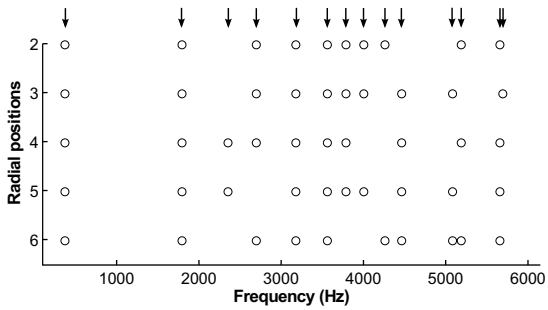


Figure 10: Natural frequencies detected for $N$=10 for radial positions 2 at 6 and at angle 60°. Frequency indications of all modes detected (↓).

The result is same for several angular positions. Figure 11 shows the detected modes from 4 angles at 1 radial position. With a robust detection ($N$=10) at several angles, 15 modes are detected with less microphones than before (5 microphones at one radius) and with a good detection distribution on frequency as well. Moreover, at radial position 4, the acoustic pressure is more energetic than the others (see Figure 4).

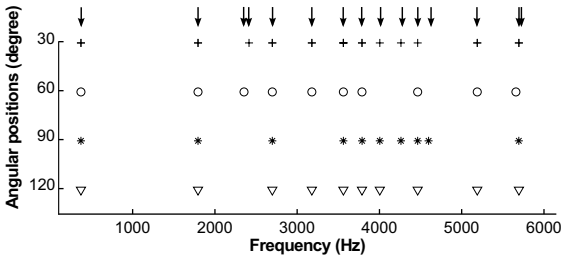


Figure 11: Natural frequencies detected for $N$=10 at the radial position 4 for the angles: 30°(+), 60° (○), 90° (∗) and 120° (▽). Frequency indications of all modes detected (↓).

The forces are then assessed from different angles. The averaged force is calculated from each angle. This allows im-

proving the force assessment. Figure 12 shows the unit force from 4 angles. The error rate is below 5%. When the force is assessed from only one position, the error rate reaches 10 %. Therefore, the robustness and the accuracy of force assessment can be improved by using several locations to measure acoustic pressure. In practice, the system will require at least two microphones at two angles and two radial positions.

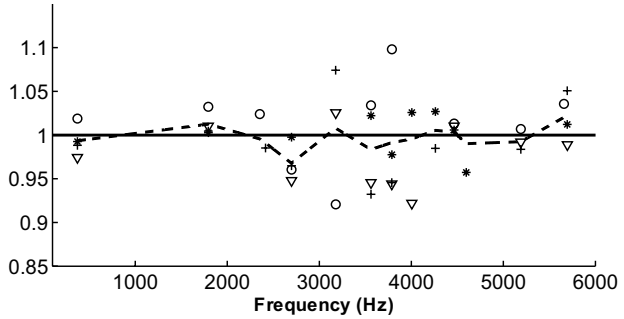


Figure 12: Unit force (—), model averaged (– – –) from dectections at radial position 4 for angles: 30°(+), 60° (∘), 90° (∗) and 120° (▽).

# 5 Conclusion and perspectives

The method to assess the force interaction between the wheel and the rail is presented. This force can be calculated from the measured pressure at near field of the surface of the wheel's web. The method is explained and validated with experimental measures. It allows assessing suitably the force.

In practice, the vibration mode shapes of the wheel will not be available. then, the on-going work focuses on the development of numerical models for the computation of the acoustic impedance and vibration response. For the impedance, the acoustic radiation of the wheel will be approximated with the Raleigh integral. The velocity of the surface of the web for each mode shape will be calculated with finite element method. Same method will be used for calculating the vibration responses between the pressure measurement point and the contact point (between the wheel and the rail). Hence, the method for estimating the contact force with acoustic pressure radiated by the wheel will be implemented on other wheels. The models will be adaptable according to simple parameters like the radius of the wheel for example.

The numerical models will enhance the post-processing (in term of computing time). The results obtained by the numerical models will be approximated by parametric equations and these parameters will be tabulated.

# References

[1] D. J Thompson, P. Fodiman, and H. Mahé. "Experimental validation of the TWINS prediction program, Part 2: resullts", *journal of sound and vibration*, **193**(1), 137-147 (1996)

[2] Official Journal of the European Communities, "Directive 2002/49/EC of the European Parliament and of the Council of 25 June 2002 relating to the assessment and management of environmental noise", *OJEC* 189/12 (2002)

[3] P. J. Remington, "Wheel/rail rolling noise, I: Theoretical analysis", *J. Acoust. Soc. Am.* **81**(6), 1805-1823 (1987)

[4] NF EN ISO 3095, "Mesurage du bruit émis par les véhicules circulantes sur rails", *AFNOR*, (2005)

[5] D. J. Ewins, *Modal testing: theory, practice and application*, Rescherch Studies Press, Philadelphia (2000)